A ROE-LIKE REFORMULATION OF THE HLLC RIEMANN SOLVER AND APPLICATIONS

Marica Pelanti

Institute of Mechanical Sciences and Industrial Applications
UMR 9219 ENSTA ParisTech-EDF-CNRS-CEA
828, Boulevard des Maréchaux, 91762 Palaiseau, France

Abstract. The Roe and HLLC Riemann solvers are widely used as building blocks of finite volume Godunov-type schemes for solving the Euler equations of gas dynamics and related hyperbolic flow models. The HLLC solver (HLL with Contact restoration) has gained increasing popularity over the last two decades since it possesses some of the good properties of the Roe solver and in addition it satisfies important entropy and positivity conditions with no need of special fixes. In the present work we rewrite the classical HLLC solver for the Euler equations in a novel form that allows an interpretation of the HLLC wave structure as an averaged system eigenstructure. This reveals a formal mathematical similarity of the HLLC solver with the Roe solver, which can be useful to extend to the HLLC method some numerical techniques devised specifically for the Roe method. We indicate several applications, focusing in particular in the present work on the design of a well-balanced HLLC method for the Euler equations with gravitational source terms.

1. **Introduction.** Finite volume Godunov-type schemes based on Riemann solvers are widely used to compute solutions to hyperbolic systems of equations. Some of the most popular approximate Riemann solvers are the solver of Roe [13] and the solver of Harten–Lax–van Leer (HLL) and its variants. The HLLC solver (HLL with Contact restoration) introduced by Toro, Spruce and Speares [15] for the Euler equations of gas dynamics has especially gained increasing popularity over the last two decades for solving a large variety of compressible flow models, since it possesses some of the good properties of the Roe solver and in addition it satisfies important entropy and positivity conditions with no need of special fixes. In the present work we rewrite the classical HLLC Riemann solver in a novel form that allows an interpretation of the HLLC wave structure as an averaged system eigenstructure. This reveals a formal mathematical similarity of the HLLC solver with the Roe solver, which can be useful to extend to the HLLC method some numerical techniques devised specifically for the Roe method. One application, which has motivated our investigation, is the extension to HLLC-type schemes of low Mach number preconditioning techniques proposed for the Roe scheme. This has been illustrated by the author in [10, 11]. In the present work we use our novel formulation of the HLLC solver to apply the f-wave approach of [1] for designing a robust well-balanced HLLC scheme for the Euler equations with gravitational source terms.

2000 *Mathematics Subject Classification.* Primary: 65M08; Secondary: 76N99.

Key words and phrases. Approximate Riemann solvers, Roe solver, HLLC solver, finite volume schemes, Euler equations, well-balanced schemes.

The author was partially funded by *Direction Générale de l'Armement* (DGA) under Grant N. 2012.60.0011.00.470.75.01.

2. **The Euler equations of gas dynamics.** The Euler equations governing an inviscid compressible flow can be written in two spatial dimensions in the conservative form:

$$\partial_t q + \partial_x f(q) + \partial_y g(q) = 0, \tag{1a}$$

where

$$q = \begin{bmatrix} \rho \\ \rho u \\ \rho v \\ E \end{bmatrix}, \quad f(q) = \begin{bmatrix} \rho u \\ \rho u^2 + p \\ \rho uv \\ u(E+p) \end{bmatrix}, \quad g(q) = \begin{bmatrix} \rho v \\ \rho vu \\ \rho v^2 + p \\ v(E+p) \end{bmatrix}. \tag{1b}$$

Here ρ is the fluid density, u and v are the flow velocity components in the x and y direction, respectively, p is the pressure, and E is the total energy per unit volume, $E = \mathcal{E} + \rho\frac{|\vec{u}|^2}{2}$, where $\mathcal{E}$ denotes the internal energy per unit volume, and $\vec{u} = (u, v)$. The system is closed through the specification of a pressure law $p = p(\mathcal{E}, \rho)$. The Euler system is hyperbolic and the eigenvalues associated to the direction $\vec{n}$, $|\vec{n}| = 1$, are $\lambda_{1,4} = \vec{u}\cdot\vec{n} \mp c$ and $\lambda_l = \vec{u}\cdot\vec{n}$ for $l = 2, 3$. The speed of sound is $c = \sqrt{\kappa h + \chi}$, where $\kappa = \frac{\partial p(\mathcal{E},\rho)}{\partial \mathcal{E}}$, $\chi = \frac{\partial p(\mathcal{E},\rho)}{\partial \rho}$, and h denotes the specific enthalpy, $h = (\mathcal{E} + p)/\rho$.

3. **Finite volume schemes based on Riemann solvers.** We briefly recall here the class of finite volume schemes based on Riemann solvers in the wave propagation formulation by LeVeque [5, 6, 7]. Let us consider a general hyperbolic system of the form

$$\partial_t q + A(q)\partial_x q + B(q)\partial_y q = 0. \tag{2}$$

We assume a spatial discretization on a Cartesian grid with cells of uniform size Δx and Δy in the x and y directions, respectively. We denote by $Q^n_{i,j}$ the approximate solution of the system at the cell (i, j), $i, j \in \mathbb{Z}$, at time t^n, $n \in \mathbb{N}$, and set $\Delta t = t^{n+1} - t^n$. The two-dimensional first-order wave propagation algorithm [5, 6] has the form

$$Q^{n+1}_{i,j} = Q^n_{i,j} - \frac{\Delta t}{\Delta x}\left(\mathcal{A}^+\Delta Q_{i-1/2,j} + \mathcal{A}^-\Delta Q_{i+1/2,j}\right) - \frac{\Delta t}{\Delta y}\left(\mathcal{B}^+\Delta Q_{i,j-1/2} + \mathcal{B}^-\Delta Q_{i,j+1/2}\right). \tag{3}$$

Here $\mathcal{A}^\pm\Delta Q$ and $\mathcal{B}^\pm\Delta Q$ are the so-called fluctuations arising from the solution of local plane-wave Riemann problems in the x and y directions, respectively [5]. To compute these quantities, a Riemann solver must be provided. Let us now consider with no loss of generality the approximation of a two-dimensional plane-wave Riemann problem in the x direction for the Euler equations, namely a Riemann problem for the system $\partial_t q + \partial_x f(q) = 0$, with initial left and right data q_ℓ and q_r. The exact solution of this problem consists of at most four constant states separated by a genuinely nonlinear 1-wave, a contact discontinuity corresponding to the eigenvalue $\lambda_2 = \lambda_3 = u$, and a genuinely nonlinear 4-wave (assuming a convex equation of state). The solution structure defined by an approximate Riemann solver can be expressed by a set of $\mathscr{M}$ waves $\mathcal{W}^l$ and corresponding speeds s^l, $\mathscr{M} \geq 2$. The so-called *f-waves* $\mathcal{Z}^l$, which carry a jump in the flux, are defined as $\mathcal{Z}^l = s^l\mathcal{W}^l$, $l = 1, \ldots, \mathscr{M}$. For conservation we require:

$$\Delta f \equiv f(q_r) - f(q_\ell) = \sum_{l=1}^{\mathscr{M}} \mathcal{Z}^l. \tag{4}$$

Once the Riemann solution structure associated to each cell pair $\{(i, j), (i+1, j)\}$ is defined, the fluctuations $\mathcal{A}^\mp\Delta Q_{i+1/2,j}$ in (3) are computed as

$$\mathcal{A}^-\Delta Q_{i+1/2,j} = \sum_{l:s^l_{i+1/2,j}\leq 0} \mathcal{Z}^l_{i+1/2,j}, \quad \mathcal{A}^+\Delta Q_{i+1/2,j} = \sum_{l:s^l_{i+1/2,j}>0} \mathcal{Z}^l_{i+1/2,j}. \tag{5}$$

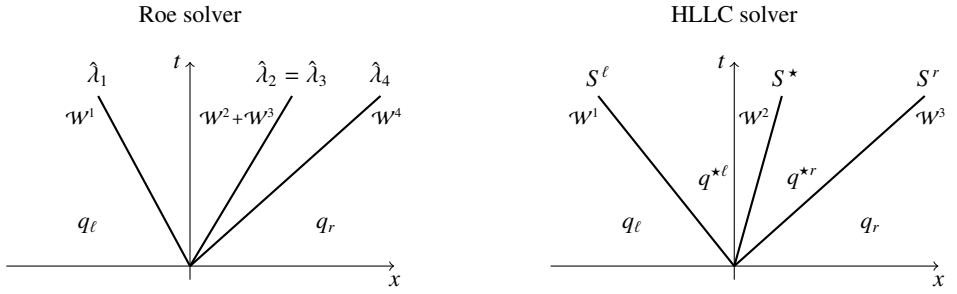

FIGURE 1. Solution structure of the Roe solver (left) and of the HLLC solver (right) for a plane-wave Riemann problem for the 2D Euler equations.

The first-order scheme (3) can be extended to second-order accuracy by adding suitable correction terms, which can be expressed again in terms of f-waves and speeds [6]. The most general form of the algorithm includes contributions from the decomposition of fluctuations in the transverse direction to account for cross-derivative terms.

3.1. **Roe approximate Riemann solver.** The idea of the approximate Riemann solver of Roe [13] is to define an approximate solution to a Riemann problem for the Euler equations $\partial_t q + \partial_x f(q) = 0$, with q and $f(q)$ as in (1), by the exact solution of a Riemann problem for a linearized system $\partial_t q + \hat{A}(q_\ell, q_r)\partial_x q = 0$. The Roe matrix $\hat{A} = \hat{A}(q_\ell, q_r)$ is defined locally by evaluating the Jacobian $A(q) = f'(q)$ of the original system in a suitable average state $\hat{q} = \hat{q}(q_\ell, q_r)$ that guarantees conservation. The Riemann solution structure of the Roe solver consists of $\mathscr{M} = 4$ waves and speeds that correspond to the eigenstructure of the Roe matrix (see Figure 1). Denoting with $\hat{r}_l$ and $\hat{\lambda}_l$ the right eigenvectors and eigenvalues of $\hat{A}$, respectively, we have $\mathcal{W}^l = \hat{\zeta}_l \hat{r}_l$ and $s^l = \hat{\lambda}_l$, $l = 1, \cdots, 4$, where $\hat{\zeta}_l$ are the coefficients of the projection of $\Delta q \equiv q_r - q_\ell$ onto the basis of the Roe eigenvectors, $q_r - q_\ell = \sum_{l=1}^{4} \hat{\zeta}_l \hat{r}_l$. The definition of the Roe eigenstructure is reported in Appendix A. The Roe numerical viscosity matrix is $\Theta = |\hat{A}|$, where $\hat{R} = [\hat{r}_1 \dots \hat{r}_4]$ and $\hat{\Lambda} = \mathrm{diag}(\hat{\lambda}_1, \dots, \hat{\lambda}_4)$.

3.2. **HLLC approximate Riemann solver.** The Riemann solution structure of the HLLC solver of Toro *et al.* [15, 14] consists of three waves $\mathcal{W}^l$, $l = 1, 2, 3$ ($\mathscr{M} = 3$), moving at speeds $s^1 = S^\ell$, $s^2 = S^\star$, $s^3 = S^r$, which separate four constant states q_ℓ, $q^{\star\ell}$, $q^{\star r}$ and q_r (see Fig. 1). In the following we will indicate with $(\cdot)_\ell$ and $(\cdot)_r$ quantities corresponding to the states q_ℓ and q_r , respectively. Moreover, we will indicate with $(\cdot)^{\star\ell}$ and $(\cdot)^{\star r}$ quantities corresponding to the states $q^{\star\ell}$ and $q^{\star r}$ adjacent, respectively on the left and on the right, to the middle wave propagating at speed $S^\star$. With this notation, the waves of the HLLC solver are $\mathcal{W}^1 = q^{\star\ell} - q_\ell$, $\mathcal{W}^2 = q^{\star r} - q^{\star\ell}$, $\mathcal{W}^3 = q_r - q^{\star r}$. We impose conservation conditions, together with the invariance of the pressure p and of the normal velocity u across the 2-wave. Then the speed $S^\star$ is determined as

$$S^\star = \frac{\Delta p + \rho_\ell u_\ell (S^\ell - u_\ell) - \rho_r u_r (S^r - u_r)}{\rho_\ell (S^\ell - u_\ell) - \rho_r (S^r - u_r)}, \tag{6}$$

where $\Delta p \equiv p_r - p_\ell$. The middle states $q^{\star\ell}$, $q^{\star r}$ are found as:

$$q^{\star\iota} = \rho_\iota \frac{S^\iota - u_\iota}{S^\iota - S^\star} \begin{bmatrix} 1 \\ S^\star \\ v_\iota \\ \frac{E_\iota}{\rho_\iota} + (S^\star - u_\iota)\left(S^\star + \frac{p_\iota}{\rho_\iota (S^\iota - u_\iota)}\right) \end{bmatrix}, \quad \iota = \ell, r. \tag{7}$$

A definition for the wave speeds must be provided. For the numerical experiments below we have adopted the definition in [3], $S^\ell = \min(u_\ell - c_\ell\,, \hat{\lambda}_1)$, $S^r = \max(u_r + c_r\,, \hat{\lambda}_4)$.

3.3. **A new formulation of the HLLC solver.** We illustrate in this Section a novel formulation of the HLLC solver that allows us to highlight a mathematical similarity with the Roe solver. First we introduce two quantities $\check{c}^\ell$, $\check{c}^r$ representing the speeds of sound associated to the external acoustic waves by defining:

$$S^\ell = u_\ell - \check{c}^\ell \qquad \text{and} \qquad S^r = u_r + \check{c}^r. \tag{8}$$

For any given choice of the estimates of the wave speeds S^ℓ and S^r the relations above determine $\check{c}^\ell$ and $\check{c}^r$. The speed $S^\star$ can be easily rewritten in terms of $\check{c}^\ell$ and $\check{c}^r$:

$$S^\star = \frac{\rho_\ell \check{c}^\ell u_\ell + \rho_r \check{c}^r u_r - \Delta p}{\rho_\ell \check{c}^\ell + \rho_r \check{c}^r}. \tag{9}$$

The densities $\rho^{\star\iota}$, $\iota = \ell, r$, corresponding to the middle states can be expressed as

$$\rho^{\star\ell} = \rho_\ell \frac{\check{c}^\ell}{S^\star - u_\ell + \check{c}^\ell} \qquad \text{and} \qquad \rho^{\star r} = \rho_r \frac{\check{c}^r}{u_r - S^\star + \check{c}^r}. \tag{10}$$

Then, after some easy algebraic manipulations, we see that the HLLC waves for the Euler equations can be equivalently rewritten as

$$\mathcal{W}^1 = \check{\zeta}_1 \check{r}_1, \quad \mathcal{W}^2 = \check{\mathcal{W}}^2 + \check{\mathcal{W}}^2_s, \;\; \check{\mathcal{W}}^2 = \check{\zeta}_2 \check{r}_2 \;\; , \check{\mathcal{W}}^2_s = \check{\zeta}_{2s} \check{r}_{2s}\,, \quad \mathcal{W}^3 = \check{\zeta}_3 \check{r}_3\,, \tag{11a}$$

where

$$\check{\zeta}_1 = \frac{\rho^{\star\ell}}{\rho_\ell \check{c}^\ell + \rho_r \check{c}^r}\left(\frac{\Delta p}{\check{c}^\ell} - \rho_r \frac{\check{c}^r}{\check{c}^\ell}\Delta u\right), \quad \check{\zeta}_3 = \frac{\rho^{\star r}}{\rho_\ell \check{c}^\ell + \rho_r \check{c}^r}\left(\frac{\Delta p}{\check{c}^r} + \rho_\ell \frac{\check{c}^\ell}{\check{c}^r}\Delta u\right), \tag{11b}$$

$$\check{\zeta}_2 = \rho^{\star r} - \rho^{\star\ell} = \Delta\rho - \left(\left(\frac{\rho^{\star\ell}}{\check{c}^\ell} + \frac{\rho^{\star r}}{\check{c}^r}\right)\Delta p + \left(\rho_\ell \rho^{\star r}\frac{\check{c}^\ell}{\check{c}^r} - \rho_r \rho^{\star\ell}\frac{\check{c}^r}{\check{c}^\ell}\right)\Delta u\right)\frac{1}{\rho_\ell \check{c}^\ell + \rho_r \check{c}^r}, \tag{11c}$$

$$\check{\zeta}_{2s} = \check{\rho}\Delta v\,, \quad \check{\rho} \equiv \frac{\rho^{\star\ell} + \rho^{\star r}}{2}\,, \quad \Delta(\cdot) \equiv (\cdot)_r - (\cdot)_\ell\,, \tag{11d}$$

and

$$\check{r}_1 = \begin{bmatrix} 1 \\ u_\ell - \check{c}^\ell \\ v_\ell \\ H_\ell - S^\star \check{c}^\ell \end{bmatrix}, \; \check{r}_3 = \begin{bmatrix} 1 \\ u_r + \check{c}^r \\ v_r \\ H_r + S^\star \check{c}^r \end{bmatrix}, \; \check{r}_2 = \begin{bmatrix} 1 \\ S^\star \\ \bar{v} \\ \Delta\check{e}^\star - \overline{\left(\frac{\chi}{\kappa}\right)} + \frac{(S^\star)^2}{2} + \overline{\left(\frac{v^2}{2}\right)} \end{bmatrix}, \; \check{r}_{2s} = \begin{bmatrix} 0 \\ 0 \\ 1 \\ \bar{v} \end{bmatrix}, \tag{11e}$$

with

$$\Delta\check{e}^\star = \frac{1}{\rho^{\star r} - \rho^{\star\ell}}\left(\rho^{\star r}\frac{c_r^2}{\kappa_r} - \rho^{\star\ell}\frac{c_\ell^2}{\kappa_\ell} - 2\check{\rho}\Delta\left(\frac{\chi}{\kappa}\right) - \Delta p + \frac{1}{2}\rho^{\star r}(u_r - S^\star)^2 - \frac{1}{2}\rho^{\star\ell}(u_\ell - S^\star)^2\right). \tag{11f}$$

Note that $\rho^{\star r}\frac{c_r^2}{\kappa_r} - \rho^{\star\ell}\frac{c_\ell^2}{\kappa_\ell} - 2\check{\rho}\Delta\left(\frac{\chi}{\kappa}\right) - \overline{\left(\frac{\chi}{\kappa}\right)}\check{\zeta}_2 = \rho^{\star r} h_r - \rho^{\star\ell} h_\ell$. Above we have denoted with $H = h + \frac{|\vec{u}|^2}{2}$ the total specific enthalpy and we have used the average operator $\bar{(\cdot)} \equiv \frac{(\cdot)_\ell + (\cdot)_r}{2}$. The expressions of the HLLC waves in this novel form reveal analogies with the waves of the Roe solver. We observe that the vectors $\check{r}_l$, like the Roe eigenvectors, have the form of the eigenvectors of the Euler system $r_l(q)$ evaluated in a special state that is a function of the left and right Riemann data (although not in the form $\hat{r}_l = r_l(\hat{q})$ as for the Roe solver), except for the quantity $\Delta\check{e}^\star$ appearing in the last component of the vector $\check{r}_2$. This quantity becomes singular if $\check{\zeta}_2 = \rho^{\star r} - \rho^{\star\ell} = 0$, which happens in the trivial case of uniform flow, $q_r = q_\ell$, but also in other cases (e.g. $p_r = p_\ell$, $\rho_\ell = \rho_r$, $u_\ell = -u_r$). Note that in such

situations the wave $\check{\mathcal{W}}^2$ is simply zero, and the Riemann solution is always well defined. For consistency we expect

$$\lim_{\rho^{\star r}-\rho^{\star \ell}\to 0} \Delta\check{e}^{\star} = 0. \tag{12}$$

Note that if the matrix $\check{R} = [\check{r}_1, \check{r}_2, \check{r}_{2s}, \check{r}_3]$ is nonsingular we can interpret the Riemann solution of the HLLC solver as the Riemann solution of a linearized system with a constant coefficient matrix $\check{A} = \check{A}(q_\ell, q_r) = \check{R}\check{\Lambda}\check{R}^{-1}$, where $\check{\Lambda} = \mathrm{diag}(u_\ell - \check{c}^{\,\ell}, S^\star, S^\star, u_r + \check{c}^{\,r})$. The HLLC numerical viscosity matrix is identified as $\Theta = |\check{A}|$.

4. **Applications.**

4.1. **Low Mach number preconditioning techniques.** The origin of the present work came from a study aimed at extending popular low Mach number preconditioning techniques for the Roe's scheme to the HLLC scheme. These techniques typically modify at low Mach number the acoustic waves and speeds that contribute to the numerical viscosity term $\sum_{l=1}^{4}(|\hat{\lambda}_l|\hat{\zeta}_l\hat{r}_l) = |\hat{A}|(q_r - q_\ell)$. Thanks to the novel formulation of the HLLC solver we were able to mimic a preconditioning technique proposed for Roe's scheme and apply it to the HLLC scheme, both for the Euler equations [11] and for a two-phase flow model [10]. We refer to [11, 10] for details.

4.2. **Well-balanced f-wave method for hyperbolic systems with source terms.** We illustrate here an application of the new form of the HLLC solver for the design of a robust well-balanced f-wave method for the Euler equations (1) with a source term $\Psi(q)$. In particular we shall consider a source term of the form $\Psi = [0, -\rho\nabla\varphi, -\rho\vec{u}\cdot\nabla\varphi]^{\mathrm{T}}$, where $\varphi(\vec{x})$ is a gravitational potential. We recall that a scheme is well-balanced if it can preserve stationary states at the discrete level and if it is able to accurately model small perturbations from steady states. In the numerical algorithm we need to solve plane-wave Riemann problems for a system of the form

$$\partial_t q + \partial_x f(q) = \psi(q), \quad \psi(q) = [0, -\rho\partial_x\varphi, 0, -\rho u\partial_x\varphi]^{\mathrm{T}}, \tag{13}$$

where $\partial_x\varphi = g\,n^{(x)}$, denoting here with $n^{(x)}$ the x-component of the unit vector $\vec{n}(\vec{x})$ indicating the direction of the gravity field $\vec{g}$. The idea of the f-wave approach [1] (see also [9]) is to include the contribution of the source term $\psi(q)$ in the jump of the fluxes that is decomposed into f-waves (cf. (4)), that is:

$$f(q_r) - f(q_\ell) - \tilde{\psi}_\Delta = \sum_{l=1}^{\mathscr{M}} \mathcal{Z}^l, \tag{14}$$

where $\tilde{\psi}_\Delta$ is a discrete interface value of the source term contribution. If this term is defined such that the discrete condition $\Delta f - \tilde{\psi}_\Delta = 0$ expresses steady conditions, and if the f-wave decomposition (14) is obtained by a projection of $\Delta f - \tilde{\psi}_\Delta$ onto a set of $\mathscr{M}$ linearly independent vectors, then we observe that steady states are maintained by the method. In fact if initially $\Delta f - \tilde{\psi}_\Delta = 0$, then the f-waves in (14) are simply zero, hence equilibrium is preserved [1, 9]. The discrete source term contribution $\tilde{\psi}_\Delta$ in (14) can be simply defined as:

$$\tilde{\psi}_\Delta = [0,\ -g\,n^{(x)}(\vec{x})\,\overline{\rho}\Delta x,\ 0,\ -g\,n^{(x)}(\vec{x})\,\overline{\rho u}\Delta x]^{\mathrm{T}}, \quad \overline{(\cdot)} \equiv \frac{1}{2}((\cdot)_\ell + (\cdot)_r). \tag{15}$$

This general definition has proven to be efficient in all the numerical tests that we have performed. If the exact steady solution is available, then we may be able to define a term $\tilde{\psi}_\Delta$ that gives an exact discrete version of the stationary conditions. For instance, let us consider the exact solution for the isothermal equilibrium in one dimension of an ideal gas

$p_0(x) = \rho_0(x) = \exp(-gx)$, $u_0(x) = 0$, which characterizes one test problem below. Then, we can take:

$$\tilde{\psi}_{\Delta} = [0, \overline{\rho \exp(g\,x)}\Delta(\exp(-g\,x)), \overline{\rho u \exp(g\,x)}\Delta(\exp(-g\,x))]^{\mathrm{T}}. \tag{16}$$

The splitting (14) can be performed by a projection onto the Roe eigenvectors, $\Delta f - \tilde{\psi}_{\Delta} = \sum_{l=1}^{4} \hat{\beta}_l \hat{r}_k$, hence we define the f-waves as $\mathcal{Z}^l = \hat{\beta}_l \hat{r}_l$, $\hat{\beta} = \hat{R}^{-1}(\Delta f - \tilde{\psi}_{\Delta})$. This f-wave Roe method (for instance used in [12]) results to be very efficient for treating sources, nonetheless it suffers from the drawbacks of the Roe method, namely unphysical states in low density regions and computation of non-entropic shocks. Note that while several entropy fixes are available for the standard Roe scheme, it might be complicated to use them within the f-wave framework (since we would need to compute the waves from the f-waves). To overcome these difficulties we apply the f-wave approach to the HLLC method, by projecting $\Delta f - \tilde{\psi}_{\Delta}$ onto the HLLC vectors $\{\check{r}_l\}_{1\le l\le 4}$. Hence we define $\mathcal{Z}^l = \check{\beta}_l \check{r}_l$, $\check{\beta} = \check{R}^{-1}(\Delta f - \tilde{\psi}_{\Delta})$. The explicit analytical expression of $\check{R}^{-1}$ can be easily obtained. To handle the problem of the singularity of $\Delta\check{e}^{\star}$ in (11f) one simple option is to set this quantity to zero if $|\check{\zeta}_2| < \epsilon$ (e.g. $\epsilon = 10^{-15}$). Another option for instance is to employ the desingularizing definition $1/\check{\zeta}_2 \triangleq 2\check{\zeta}_2/(\check{\zeta}_2^2 + \max(\check{\zeta}_2^2, \epsilon^2))$ [4].

4.2.1. *Numerical experiments.* All the tests are performed with second-order algorithms, MC limiter, Courant number = 0.9. We assume an ideal gas with $\gamma = 1.4$ and we set $g = 1$.

Riemann problems. We solve two Riemann problems to show the advantages of the f-wave HLLC method with respect to the f-wave Roe method. The computational domain is $[0, 1]$ and the initial discontinuity is at $x = 0.5$. Free flow boundary conditions are used. First, we solve a problem with $\rho_\ell = 3$, $\rho_r = 1$, $p_\ell = 3$, $p_r = 1$, $u_\ell = u_r = 0.9$. The solution contains a left-going transonic rarefaction, which is computed correctly by the HLLC method but not by the Roe method, which would need an entropy fix. See Fig. 2, left plot. The second test is a version with gravity of the double rarefaction test of [3]. Here $\rho_\ell = \rho_r = 1$, $p_\ell = p_r = 0.4$, $u_r = -u_\ell = 2$. The solution involves two rarefactions going in opposite directions that form a region of very low density and pressure in between. The Roe scheme fails for this test, whereas the HLLC scheme computes the solution with no difficulties (note that gravity here pulls slightly toward the left). See Fig. 3, left plot. Results for a double rarefaction test in two dimensions are displayed in Fig. 3, right plot. Here we have a setup analogous to the 1D test, with initial discontinuity at $x = 1$ in the domain $[0, 2] \times [0, 2]$. Gravity acts downwards along the y axis. Top and bottom boundaries are walls.

Perturbation of isothermal equilibrium. We perform a one-dimensional test proposed in [8] to investigate the well-balanced property of the method. A small perturbation of the isothermal equilibrium conditions $p_0(x) = \rho_0(x) = \exp(-gx)$, $u_0(x) = 0$, is considered for the pressure field: $p(x)|_{t=0} = p_0(x) + \eta \exp(-100(x - 0.5)^2)$, $\eta = 10^{-4}$, $x \in [0, 1]$. The f-wave HLLC method exhibits the same good behavior of the f-wave Roe method, see Fig. 2, right plot, and results are qualitatively similar to those in the literature [8, 16, 2].

Radial Rayleigh–Taylor instability. We perform the two-dimensional Rayleigh–Taylor instability test proposed in [8] (with initial conditions as in [2]). Here we consider a radial gravitational potential (gravity is directed inward, $\varphi = g|\vec{x}|$). A radially symmetric isothermal equilibrium is assumed, for which the pressure is continuous across $|\vec{x}| = r_0 = 0.6$ but has a density jump $\Delta_\rho = 0.1$ across $|\vec{x}| = r_0(1 + \eta\cos(\xi\theta))$, $\xi = 20$, $\eta = 0.02$. Results are shown in Figure 4 for a second-order computation on the domain $[-1, 1] \times [-1, 1]$ with 240×240 grid cells. As expected we see Rayleigh–Taylor instabilities arise at the interface with the density jump. Elsewhere equilibrium conditions are well maintened, and results are analogous to [8].

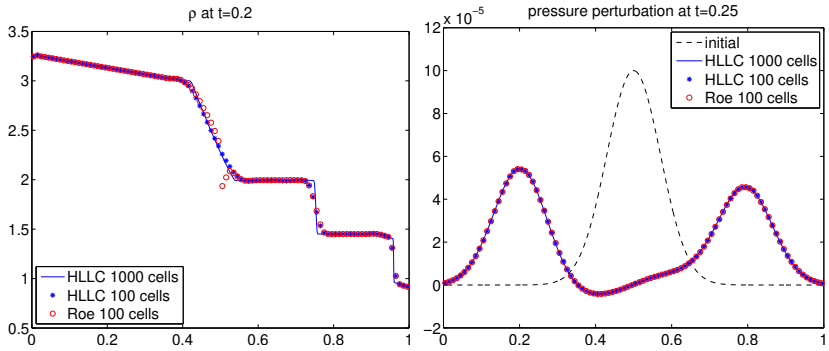

FIGURE 2. Left: Transonic rarefaction test with gravity ($\varphi = gx$), ρ at $t = 0.2$. Right: Perturbation of isothermal equilibrium test. $p(x,t) - p_0(x)$ at $t = 0.25$. HLLC ($*$), Roe ($\circ$) results with 100 cells, HLLC results with 1000 cells ($-$).

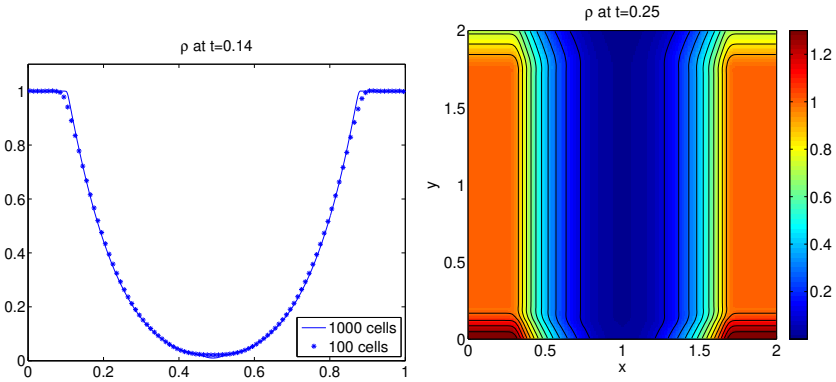

FIGURE 3. Double rarefaction test with gravity computed by the HLLC method. Left: 1D test ($\varphi = gx$), ρ at $t = 0.14$, results with 100 cells ($*$) and 1000 cells ($-$). Right: 2D test ($\varphi = gy$), ρ at $t = 0.25$, results with 200×200 cells.

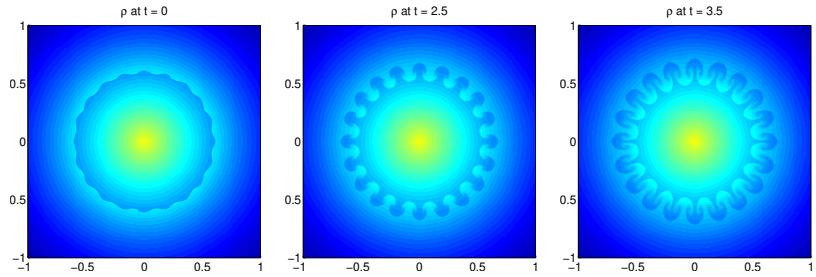

FIGURE 4. Rayleigh–Taylor instability test. 2nd order HLLC method, 240×240 cells. Density at $t = 0,\ 2.5,\ 3.5$. Color scale from 0.2 (darker) to 1.5 (lighter).

5. **Conclusions.** We have presented a reformulation of the HLLC Riemann solver, which shows that the HLLC wave structure can be interpreted as an averaged system eigenstructure. In particular, we use this new Roe-like form of the HLLC solver to develop a robust second-order well-balanced f-wave HLLC method for the solution of the Euler

equations with gravitational source terms. The presented reformulation of the HLLC solver can be used for other applications [11], and it could be derived also for more complex flow models, see e.g. [10].

Appendix A. **Roe eigenstructure for the Euler equations.** We recall the eigenstructure of the Roe matrix $\hat{A}(q_\ell, q_r)$ for a plane-wave Riemann problem in the x direction with data q_ℓ, q_r for the Euler equations. We assume κ, χ = constant. We introduce the averages:

$$\hat{a} = \frac{a_\ell\sqrt{\rho_\ell}+a_r\sqrt{\rho_r}}{\sqrt{\rho_\ell}+\sqrt{\rho_r}},\ a = u, v, H, \quad \hat{\rho} = \sqrt{\rho_\ell\rho_r}, \quad \hat{c} = \sqrt{\kappa(\hat{H} - \hat{\mathcal{K}}) + \chi}, \quad \hat{\mathcal{K}} = \frac{\hat{u}^2+\hat{v}^2}{2}. \tag{17}$$

The Roe eigenvalues are $\hat{\lambda}_1 = \hat{u} - \hat{c}$, $\hat{\lambda}_2 = \hat{\lambda}_3 = \hat{u}$, $\hat{\lambda}_4 = \hat{u} + \hat{c}$. The matrix $\hat{R} = [\hat{r}_1, \ldots, \hat{r}_4]$ of the corresponding Roe right eigenvectors is

$$\hat{R} = \begin{pmatrix} 1 & 1 & 0 & 1 \\ \hat{u} - \hat{c} & \hat{u} & 0 & \hat{u} + \hat{c} \\ \hat{v} & \hat{v} & 1 & \hat{v} \\ \hat{H} - \hat{u}\hat{c} & -\frac{\chi}{\kappa} + \hat{\mathcal{K}} & \hat{v} & \hat{H} + \hat{u}\hat{c} \end{pmatrix}. \tag{18}$$

The coefficients $\hat{\zeta}_l$, $l = 1, \ldots 4$, of the Roe eigen-decomposition $q_r - q_\ell = \sum_{l=1}^4 \hat{\zeta}_l\hat{r}_l$, are:

$$\hat{\zeta}_1 = \frac{1}{2\hat{c}}\left(\frac{\Delta p}{\hat{c}} - \hat{\rho}\,\Delta u\right), \quad \hat{\zeta}_2 = \Delta\rho - \frac{\Delta p}{\hat{c}^2}, \quad \hat{\zeta}_3 = \hat{\rho}\Delta v, \quad \hat{\zeta}_4 = \frac{1}{2\hat{c}}\left(\frac{\Delta p}{\hat{c}} + \hat{\rho}\,\Delta u\right). \tag{19}$$

REFERENCES

[1] D. Bale, R. J. LeVeque, S. Mitran and J. A. Rossmanith, A wave-propagation method for conservation laws and balance laws with spatially varying flux functions, *SIAM J. Sci. Comput.*, **24** (2002), 955–978.

[2] P. Chandrashekaand and C. Klingenberg, A second-order well-balanced finite volume scheme for Euler equations with gravity, *SIAM J. Sci. Comput.*, **37** (2018), B382–B402.

[3] B. Einfeldt, C. D. Munz, P. L. Roe and B. Sjögreen, On Godunov-type methods near low densities, *J. Comput. Phys.*, **92** (1991), 273–295.

[4] A. Kurganov and G. Petrova, A second-order well-balanced positivity preserving central-upwind scheme for the Saint-Venant system, *Commun. Math. Sci.*, **5** (2007), 133–160.

[5] R. J. LeVeque, Wave propagation algorithms for multi-dimensional hyperbolic systems, *J. Comput. Phys.*, **131** (1997), 327–353.

[6] R. J. LeVeque, *Finite Volume Methods for Hyperbolic Problems*, Cambridge University Press, 2002.

[7] R. J. LeVeque, CLAWPACK Software, `http://www.clawpack.org`.

[8] R. J. LeVeque and D. S. Bale, Wave-Propagation Methods for Conservation Laws with Source Terms, in *Proc. of the 7th Intl. Conf. on Hyperbolic Problems*, (Ed. R. Jeltsch), Birkhäuser Verlag (1998), 609–618.

[9] R. J. LeVeque and M. Pelanti, A class of approximate Riemann solvers and their relation to relaxation schemes, *J. Comput. Phys.*, **172** (2001), 572–591.

[10] M. Pelanti, Low Mach number preconditioning techniques for Roe-type and HLLC-type methods for a two-phase compressible flow model, *Appl. Math. Comp.*, **310** (2017), 112–133.

[11] M. Pelanti, Wave structure similarity of the HLLC and Roe Riemann solvers: Application to low Mach number preconditioning, *SIAM J. Sci. Comput.*, **40** (2018), A1836–A1859.

[12] M. Pelanti and R. J. LeVeque, High-Resolution Finite Volume Methods for dusty gas jets and plumes, *SIAM J. Sci. Comput.*, **28** (2006), 1335–1360.

[13] P. L. Roe, Approximate Riemann solvers, parameter vectors, and difference schemes, *J. Comput. Phys.*, **43** (1981), 357–372.

[14] E. F. Toro, *Riemann Solvers and Numerical Methods for Fluid Dynamics*, Springer-Verlag, 1997.

[15] E. F. Toro, M. Spruce and W. Speares, Restoration of the contact surface in the HLL Riemann solver, *Shock Waves*, **4** (1994), 25–34.

[16] Y. Xing and C.-W. Shu, High Order Well-Balanced WENO Scheme for the Gas Dynamics Equations Under Gravitational Fields, *J. Sci. Comput.*, **54** (2013), 645–662.

Received xxxx 20xx; revised xxxx 20xx.

E-mail address: `marica.pelanti@ensta-paristech.fr`